Energy loss to conductors operated at lineal current densities ≤ 10 MA/cm: Semianalytic model, magnetohydrodynamic simulations, and experiment

W. A. Stygar,[1] S. E. Rosenthal,[1] H. C. Ives,[2] T. C. Wagoner,[3] G. O. Allshouse,[1] K. E. Androlewicz,[3] G. L. Donovan,[1] D. L. Fehl,[1] M. H. Frese,[4] T. L. Gilliland,[3] M. F. Johnson,[5] J. A. Mills,[1] D. B. Reisman,[6] P. G. Reynolds,[5] C. S. Speas,[1] R. B. Spielman,[3] K. W. Struve,[1] A. Toor,[6] and E. M. Waisman[1]

[1]*Sandia National Laboratories, Albuquerque, New Mexico 87185, USA*
[2]*EG&G, Albuquerque, New Mexico 87107, USA*
[3]*Ktech Corporation, Albuquerque, New Mexico 87123, USA*
[4]*NumerEx, Albuquerque, New Mexico 87106, USA*
[5]*Team Specialty Products Corporation, Albuquerque, New Mexico 87123, USA*
[6]*Lawrence Livermore National Laboratory, Livermore, California 94550, USA*

(Received 29 April 2008; published 8 December 2008)

We have developed a semianalytic expression for the total energy loss to a vacuum transmission-line electrode operated at high lineal current densities. (We define the lineal current density $j_\ell \equiv B/\mu_0$ to be the current per unit electrode width, where B is the magnetic field at the electrode surface and μ_0 is the permeability of free space.) The expression accounts for energy loss due to Ohmic heating, magnetic diffusion, $\mathbf{j} \times \mathbf{B}$ work, and the increase in the transmission line's vacuum inductance due to motion of the vacuum-electrode boundary. The sum of these four terms constitutes the Poynting fluence at the original location of the boundary. The expression assumes that (i) the current distribution in the electrode can be approximated as one-dimensional and planar; (ii) the current $I(t) = 0$ for $t < 0$, and $I(t) \propto t$ for $t \geq 0$; (iii) $j_\ell \leq 10$ MA/cm; and (iv) the current-pulse width is between 50 and 300 ns. Under these conditions we find that, to first order, the total energy lost per unit electrode-surface area is given by $W_t(t) = \alpha t^\beta B^\gamma(t) + \zeta t^\kappa B^\lambda(t)$, where $B(t)$ is the *nominal* magnetic field at the surface. The quantities α, β, γ, ζ, κ, and λ are material constants that are determined by normalizing the expression for $W_t(t)$ to the results of 1D magnetohydrodynamic MACH2 simulations. For stainless-steel electrodes operated at current densities between 0.5 and 10 MA/cm, we find that $\alpha = 3.36 \times 10^5$, $\beta = 1/2$, $\gamma = 2$, $\zeta = 4.47 \times 10^4$, $\kappa = 5/4$, and $\lambda = 4$ (in SI units). An *effective* time-dependent resistance, appropriate for circuit simulations of pulsed-power accelerators, is derived from $W_t(t)$. Resistance-model predictions are compared to energy-loss measurements made with stainless-steel electrodes operated at peak lineal current densities as high as 12 MA/cm (and peak currents as high as 23 MA). The predictions are consistent with the measurements, to within experimental uncertainties. We also find that a previously used electrode-energy-loss model overpredicts the measurements by as much as an order of magnitude.

DOI: 10.1103/PhysRevSTAB.11.120401 PACS numbers: 84.70.+p, 84.32.Ff, 84.37.+q, 72.15.−v

I. INTRODUCTION

High-current pulsed-power accelerators, such as the 20-MA Z machine [1–10] and the proposed 60-MA accelerators outlined in Ref. [11], are designed to deliver a high-current pulse to a load with spatial dimensions on the order of 1 cm. The current is typically delivered to the load by a system of self-magnetically insulated transmission lines (MITLs) [1,2,4,9,10].

A MITL is a vacuum transmission line that operates at an electric field sufficiently high to cause electrons to be emitted from the MITL's cathode, and at a magnetic field sufficiently high to prevent most of the emitted electrons from striking the anode [12–16]. MITLs are commonly used in pulsed-power accelerators to transmit electromagnetic power and energy to a load [17–20]. An idealized representation of a one-dimensional (1D) steady-state MITL is given by Fig. 1 [16]. In the steady state, the free electron current (i.e., the electron current in the vacuum gap) flows approximately parallel to both the anode and cathode electrodes [12–16]. The magnitude of the bound current in the anode I_a is greater than the bound cathode current I_k, since $I_a = I_k + I_f$, where I_f is the free electron current, which is commonly referred to as the electron-flow current.

Optimizing the design and performance of a pulsed-power accelerator requires an understanding of how the conductors of its MITL system perform when operated at high lineal current densities. More specifically, it is required to understand how much energy is lost to such conductors as a function of time. We define the lineal current density j_ℓ to be the current per unit conductor width; hence $j_\ell \equiv B/\mu_0$ where B is the magnetic field at the conductor surface and μ_0 is the permeability of free space. (SI units are used for equations throughout.) The *lineal* current density is to be distinguished from the *areal*

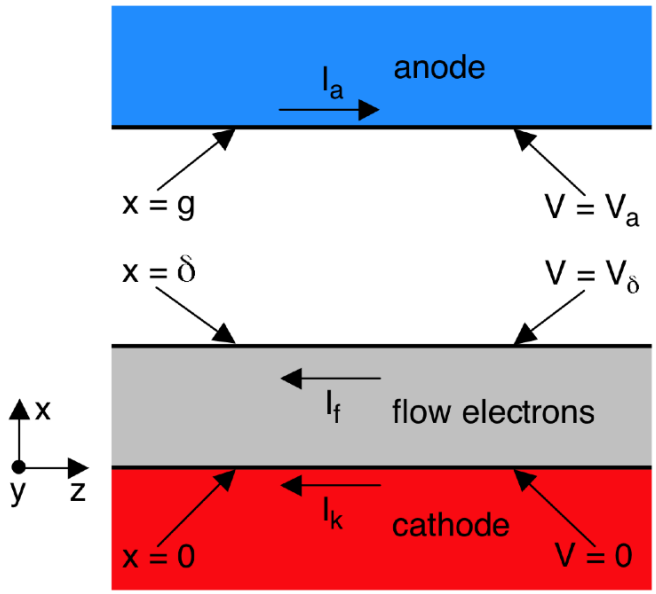

FIG. 1. (Color) Idealized 1D magnetically insulated transmission line (MITL) in planar geometry [16]. This figure assumes that the electromagnetic power flows in the positive-z direction. The electric- and magnetic-field vectors point in the negative-x and negative-y directions, respectively. The quantity g is the anode-cathode gap, δ is the thickness of the electron sheath, I_a is the magnitude of the bound anode current, I_f is the electron-flow current, I_k is the bound cathode current, V_a is the total MITL voltage, and V_δ is the voltage at the edge of the sheath.

current density; i.e., the current per unit conductor area. As suggested by Fig. 1, the lineal current densities of interest in a MITL are those at the MITL's anode and cathode surfaces, and depend on I_a and I_k, respectively. When a MITL is well insulated, $I_a \sim I_k$ [12–16].

The calculations presented in Refs. [17–20] suggest that a peak value of j_ℓ on the order of 10 MA/cm, with a pulse width on the order of 100 ns, may be required to achieve z-pinch-driven thermonuclear fusion. Similar current densities may also be required for advanced equation-of-state, radiation-physics, radiation-effects, astrophysics, and other high-energy-density-physics experiments.

The total energy loss associated with the operation of a conductor at such lineal current densities has four principal components: (i) Ohmic heating of the conductor [21–23]; (ii) diffusion of magnetic field into the conductor [21–23]; (iii) $\mathbf{j} \times \mathbf{B}$ work performed on the conductor [23]; and (iv) the energy loss associated with an increase in vacuum inductance due to motion of the vacuum-conductor boundary. The sum of these four terms constitutes the Poynting fluence at the original location of the boundary.

Analytic calculations of the Ohmic and magnetic-diffusion losses under various conditions are presented by Knoepfel in Refs. [21,22]. The Knoepfel results are applied by Singer and Hunter [23] to *copper* conductors operated at high lineal current densities. The Singer-Hunter calculations assume that the resistivity η of copper is proportional to the temperature θ, which implies that the Ohmic and diffusive losses scale as B^3. This approximation is valid at near-solid densities (9 g/cm^3) and temperatures $\leq 1080°$C. Such temperatures correspond to peak lineal current densities ≤ 0.7 MA/cm [21,22,24]. (In Appendix A, we give Knoepfel's relation for the increase in the conductor-surface temperature as a function of the peak lineal current density [21,22].)

The approximation $\eta \propto \theta$ is, however, not applicable at higher temperatures. In particular, at densities $\sim$9 g/cm^3, the resistivity of copper is expected to be relatively *constant* for temperatures between 10 000 and 30 000 K, with a value on the order of 100 $\mu\Omega$-cm [25,26]. This is consistent with Fig. 10.23 of Ref. [21], which suggests that the resistivity of solid-density copper peaks at $\sim$100 $\mu\Omega$-cm, over a similar temperature range. Hence, at lineal current densities significantly in excess of 0.7 MA/cm, the B^3 scaling assumed by the Singer-Hunter model of Ohmic and magnetic-diffusion losses is not quite applicable.

Singer and Hunter [23] also estimate the energy loss due to $\mathbf{j} \times \mathbf{B}$ work performed on a copper conductor, using results presented by Knoepfel [21,22]. Estimates are given in weak- and strong-magnetic-field limits, and assume that the magnetic field at the surface of the conductor has a step-function time history. Figure 1 of Ref. [23] plots the sum of Ohmic, magnetic-diffusion, and $\mathbf{j} \times \mathbf{B}$ losses as a function of time. This figure is, however, not self-consistent, since the Ohmic and diffusive components assume that the current increases as $t^{1/2}$, whereas for the $\mathbf{j} \times \mathbf{B}$ component, the current time history is assumed to be a step function.

Even though copper has a significantly lower room-temperature resistivity than stainless steel, the conductors of MITLs in pulsed-power accelerators are often fabricated from stainless, which has high-voltage, vacuum, fabrication, and mechanical properties superior to those of copper and many other materials [27]. At near-solid densities ($\sim$ 8 g/cm^3) and temperatures between 4000 and 30 000 K, the resistivity of stainless steel is, like copper, expected to be relatively constant, with a value on the order of 100 $\mu\Omega$-cm [26].

In this article, we develop a semianalytic model of the total energy loss to a conductor operated at peak lineal current densities as high as 10 MA/cm, for current pulse widths between 50 and 300 ns. The model does not assume that the resistivity is proportional to the temperature; but rather that for current densities and time scales at which most of the energy loss occurs, the resistivity can be approximated as a constant. The model accounts for the Ohmic, magnetic-diffusion, and $\mathbf{j} \times \mathbf{B}$ energy losses in a self-consistent manner. The model also accounts for the loss associated with the vacuum-inductance increase due to motion of the vacuum-conductor boundary, a loss mechanism not considered in Refs. [21–23]. As shown in this article, this loss can be a factor of 2 greater than the $\mathbf{j} \times \mathbf{B}$ loss.

The semianalytic model is developed in Sec. II. In Sec. III we express the model in terms of an *effective* resistance that can be used in circuit simulations of the operation of pulsed-power accelerators. In Sec. IV, we normalize the expressions developed in Secs. II and III to results of numerical 1D magnetohydrodynamic (MHD) simulations of a stainless-steel conductor subjected to high lineal current densities. The simulations were performed using MACH2, a $2\frac{1}{2}$D MHD simulation code [28]. The simulations extend the work presented by Rosenthal and colleagues in Ref. [26], and complement simulations performed by Spielman, Chantrenne, and McDaniel [29]. A description of the MACH2 model can be found in [26,28]. The simulations use the electrical and thermal conductivities discussed in [30] and the equation-of-state tables presented in [31]. In Sec. V we describe measurements, which were performed on the Z accelerator, of the energy loss to stainless-steel conductors [32]. In Sec. VI we compare the measurements with predictions of the semianalytic model, and those of a model previously used by the pulsed-power community. Suggestions for future work are discussed in Sec. VII.

The expression we develop in Sec. III for the effective resistance of a conductor is most accurate at high lineal current densities; low current densities are discussed in Appendix A. The conductor-energy-loss model previously used by the pulsed-power community is outlined in Appendix B. The comparison in Sec. VI between measurements and predictions implicitly assumes that the current-density profiles of the experimental configurations described in Sec. V are 1D and planar; Appendix C examines this assumption. The comparison in Sec. VI also assumes that the time history of the current applied to the experimental hardware can be approximated as a linear ramp; this assumption is examined in Appendix D.

II. SEMIANALYTIC MODEL OF THE TOTAL ENERGY LOSS TO A CONDUCTOR

In this section we develop a semianalytic expression for the total energy loss to a conductor operated at high lineal current densities. The model makes a number of simplifying assumptions, and hence is accurate only to first order.

The total energy loss (per unit conductor-surface area) W_t is assumed to be the sum of four components:

$$W_t = W_r + W_m + W_w + W_{\Delta L}, \tag{1}$$

where W_r is the loss due to resistive (i.e., Ohmic) heating, W_m is the energy of the magnetic field that has diffused into the conductor, W_w is the $\mathbf{j} \times \mathbf{B}$ work performed throughout the conductor, and $W_{\Delta L}$ is the energy required by the change in vacuum inductance due to motion of the vacuum-conductor boundary.

We consider the case where the total current $I(t)$ applied to a conductor is a linear function of time:

$$I(t) = 0 \quad \text{when } t < 0; \tag{2}$$

$$I(t) \propto t \quad \text{when } t \geq 0. \tag{3}$$

Although there are an infinite number of possible current waveforms, we restrict our analysis in this article to such a linear ramp. This allows us to use results presented earlier by Knoepfel [21,22], and to simplify our semianalytic model. (It is straightforward to apply the approach presented herein to other power-law functions.) When Eqs. (2) and (3) are a reasonable approximation to the current time history, and the resistivity of the conductor can be approximated as a constant, then as shown by Knoepfel [21,22]

$$W_r + W_m = \frac{4}{5\pi^{1/2}\mu_0^{3/2}}(\eta t)^{1/2} B^2(t), \tag{4}$$

where η is the resistivity of the conductor and $B(t)$ is the magnetic field at the conductor *surface*.

We do not develop analytic expressions for W_w and $W_{\Delta L}$, which would be outside the scope of this article; we instead estimate upper bounds for these quantities. To obtain an upper bound for W_w we assume a snowplow model: we assume that (i) the magnetic pressure at the conductor surface is significantly greater than that inside; (ii) material-strength effects can be neglected; (iii) the mass density of the conductor before it is compressed is approximately given by its room-temperature value; and (iv) the magnetic pressure snowplows the conductor mass as it is accelerated. Under these simplifying assumptions

$$W_w \sim \int \frac{B^2(t)}{2\mu_0} dx = \int \frac{B^2(t)}{2\mu_0} v dt, \tag{5}$$

where

$$\frac{B^2(t)}{2\mu_0} = \frac{d}{dt}(mv), \tag{6}$$

$$m = \rho_0 \int v dt. \tag{7}$$

In these expressions v is the characteristic inward velocity of the total accreted mass, m is the accreted mass per unit area, and ρ_0 is the initial room-temperature mass density of the conductor. Combining Eqs. (2), (3), and (5)–(7) gives

$$W_w = \left(\frac{1}{192\rho_0\mu_0^3}\right)^{1/2} t B^3(t). \tag{8}$$

The energy loss (per unit conductor-surface area) due to the increase in vacuum inductance $W_{\Delta L}$ is approximately given by

$$W_{\Delta L} \sim \frac{B^2(t)}{2\mu_0} \int v dt. \tag{9}$$

Combining Eqs. (2), (3), (6), (7), and (9), one obtains an upper bound on $W_{\Delta L}$:

$$W_{\Delta L} = \left(\frac{1}{48\rho_0\mu_0^3}\right)^{1/2} tB^3(t). \tag{10}$$

We note that

$$W_{\Delta L} = 2W_w. \tag{11}$$

It follows from Eqs. (8) and (10) that

$$W_w + W_{\Delta L} = \left(\frac{3}{64\rho_0\mu_0^3}\right)^{1/2} tB^3(t). \tag{12}$$

Equations (4) and (12) suggest that, in general,

$$W_r + W_m = \alpha t^\beta B^\gamma(t), \tag{13}$$

$$W_w + W_{\Delta L} = \zeta t^\kappa B^\lambda(t), \tag{14}$$

$$W_t = \alpha t^\beta B^\gamma(t) + \zeta t^\kappa B^\lambda(t), \tag{15}$$

where α, β, γ, ζ, κ, and λ are material constants. In this article we determine the constants for a stainless-steel conductor by normalizing Eqs. (13) and (14) to the results of 1D MACH2 simulations.

III. EFFECTIVE RESISTANCE OF A CONDUCTOR SYSTEM

We develop below an expression for an *effective* resistance $R_{\rm eff}$ of a system of conductors operated at high lineal current densities. The expression can be used to account for conductor-energy-loss effects in circuit simulations of the operation of a pulsed-power accelerator. As shown below, $R_{\rm eff}$ is nonlinear since it is a function of $I(t)$.

Following Parks and Spence [33], we obtain an effective resistance by equating the time-rate-of-change of W_t to an Ohmic power loss:

$$\frac{\partial}{\partial t}\int_S W_t dA = I^2 R_{\rm eff}, \tag{16}$$

where S is the total surface area of the system of conductors. Combining Eqs. (2), (3), (15), and (16), and assuming that the conductor system is cylindrically symmetric so that

$$B(t) = \frac{\mu_0 I(t)}{2\pi r} \tag{17}$$

(where r is the distance from the symmetry axis), we obtain

$$R_{\rm eff}(t) = X_1 t^{\beta-1} I^{\gamma-2}(t)\int_S \frac{dA}{r^\gamma} + X_2 t^{\kappa-1} I^{\lambda-2}(t)\int_S \frac{dA}{r^\lambda}, \tag{18}$$

where

$$X_1 \equiv \alpha(\beta+\gamma)\left(\frac{\mu_0}{2\pi}\right)^\gamma, \tag{19}$$

$$X_2 \equiv \zeta(\kappa+\lambda)\left(\frac{\mu_0}{2\pi}\right)^\lambda. \tag{20}$$

Assuming that the conductor system consists of cylindrical and radial-disk conductors, we obtain from Eq. (18) the following:

$$R_{\rm eff} = R_{\rm cyl} + R_{\rm disk}, \tag{21}$$

where

$$R_{\rm cyl} = 2\pi X_1 t^{\beta-1} I^{\gamma-2}(t)\sum_i\left(\frac{\ell_i}{a_i^{\gamma-1}}\right) + 2\pi X_2 t^{\kappa-1} I^{\lambda-2}(t)\sum_i\left(\frac{\ell_i}{a_i^{\lambda-1}}\right), \tag{22}$$

$$R_{\rm disk} = \frac{2\pi X_1 t^{\beta-1} I^{\gamma-2}(t)}{2-\gamma}\sum_j \sec\vartheta_j (c_j^{2-\gamma} - b_j^{2-\gamma}) + \frac{2\pi X_2 t^{\kappa-1} I^{\lambda-2}(t)}{2-\lambda}\sum_j \sec\vartheta_j (c_j^{2-\lambda} - b_j^{2-\lambda}). \tag{23}$$

The first term on the right-hand sides of Eqs. (22) and (23) is due to $W_j + W_m$; the second term is due to $W_w + W_{\Delta L}$. The quantities ℓ_i and a_i are the length and radius of the ith cylindrical electrode, respectively. The quantities c_j and b_j are the outer and inner radii of the jth disk electrode, and ϑ_j is the angle made by the jth disk electrode with respect to the horizontal.

For the special case when $\gamma = 2$, Eq. (23) becomes

$$R_{\rm disk} = 2\pi X_1 t^{\beta-1}\sum_j \sec\vartheta_j\left[\ln\left(\frac{c_j}{b_j}\right)\right] + \frac{2\pi X_2 t^{\kappa-1} I^{\lambda-2}(t)}{2-\lambda}\sum_j \sec\vartheta_j (c_j^{2-\lambda} - b_j^{2-\lambda}). \tag{24}$$

A similar result is obtained for the second term on the right-hand side of Eq. (23) when $\lambda = 2$.

IV. 1D MHD MACH2 SIMULATIONS

We have calculated numerically the energy loss to a stainless-steel conductor operated at high-lineal-current densities by performing 1D MHD simulations using the MACH2 code [28]. The simulations incorporate Lee-More-Desjarlais electrical and thermal conductivities [30] and SESAME equation-of-state tables [31]. The simulations use Lagrangian coordinates, and apply a linear-ramp current pulse to a solid stainless-steel cylinder that has an initial radius of 1 cm. The initial grid spacing and time step used are 3 μm and 1 ps, respectively. The simulations conserve energy to within 0.002%. When test simulations are performed with the resistivity held constant in MACH2, the simulation results agree with the predictions of the Knoepfel relation [Eq. (4)] to within 1% (when $\mathbf{j}\times\mathbf{B}$

work can be neglected). A more complete description of the MHD simulations will be presented in a companion article by Rosenthal and colleagues [34].

Twenty MACH2 simulations were performed. These reach peak currents that range from 3.14 to 62.8 MA; hence the *nominal* peak lineal-current densities range from 0.5 to 10 MA/cm. (The *actual* peak current densities are somewhat higher than the nominal values because the cylinder is compressed slightly by the magnetic field.) The simulations reach peak current in times that range from 50 to 300 ns. Results of the simulations are summarized by Table I.

The results are used to estimate the values of the six material constants of Eqs. (13) and (14) in the following manner: The constants β and γ are obtained from a linearized least-squares fit to Eq. (13) of the results listed in the first three columns of Table I. To within the uncertainties of the fit, $\beta = 1/2$ and $\gamma = 2$. Assuming these values, we find that for the results listed, the average value of $\alpha = 3.36 \times 10^5$. Hence,

$$\alpha = 3.36 \times 10^5, \tag{25}$$

$$\beta = 1/2, \tag{26}$$

$$\gamma = 2. \tag{27}$$

Similarly, Eq. (14) and columns 1, 2, and 5 of Table I are used to find that

$$\zeta = 4.47 \times 10^4, \tag{28}$$

$$\kappa = 5/4, \tag{29}$$

$$\lambda = 4. \tag{30}$$

Consequently,

$$W_r + W_m = (3.36 \times 10^5) t^{1/2} B^2(t), \tag{31}$$

$$W_w + W_{\Delta L} = (4.47 \times 10^4) t^{5/4} B^4(t), \tag{32}$$

$$W_t = (3.36 \times 10^5) t^{1/2} B^2(t) + (4.47 \times 10^4) t^{5/4} B^4(t). \tag{33}$$

Equations (25)–(33) are, of course, most accurate for the rise times and peak lineal current densities considered by Table I, when the conductor is a 1-cm-radius solid stainless-steel cylinder.

Table I compares the values at peak current of $W_r + W_m$, $W_w + W_{\Delta L}$, and W_t as predicted by the semianalytic model [Eqs. (31)–(33)] to those predicted by MACH2. For the 20

TABLE I. Summary of conductor-energy-loss calculations. These assume a linear-ramp current pulse is applied to a 1-cm-radius solid cylinder of stainless steel. The numerical results are obtained from 1D Lagrangian MHD simulations performed using the MACH2 code [28,30,31]. The losses presented are those obtained at peak current. The expression for $W_w + W_{\Delta L}$ given by Eq. (32) predicts a loss that disagrees with the numerical result for many of the conditions considered, but the disagreements occur when the magnitude of this component is significantly less than that of $W_r + W_m$. As suggested by the last three columns, the total energy loss W_t given by Eq. (33) agrees to first order with the simulation results.

Time to peak current (ns)	Peak nominal lineal current density (MA/cm)	$W_r + W_m$ (MACH2) (J/m^2)	$W_r + W_m$ [Eq. (31)] (J/m^2)	$W_w + W_{\Delta L}$ (MACH2) (J/m^2)	$W_w + W_{\Delta L}$ [Eq. (32)] (J/m^2)	W_t (MACH2) (J/m^2)	W_t [Eq. (33)] (J/m^2)	Difference between the semianalytic and MACH2 estimates of W_t
50	0.5	2.66×10^5	2.97×10^5	-3.70×10^2	5.21×10^2	2.65×10^5	2.97×10^5	12%
50	1	1.18×10^6	1.19×10^6	-9.29×10^3	8.33×10^3	1.17×10^6	1.19×10^6	2%
50	2	4.87×10^6	4.75×10^6	-1.43×10^5	1.33×10^5	4.72×10^6	4.88×10^6	3%
50	5	3.40×10^7	2.97×10^7	8.55×10^5	5.21×10^6	3.49×10^7	3.49×10^7	0%
50	10	1.20×10^8	1.19×10^8	8.34×10^7	8.33×10^7	2.04×10^8	2.02×10^8	−1%
100	0.5	3.79×10^5	4.19×10^5	-1.97×10^1	1.24×10^3	3.79×10^5	4.21×10^5	11%
100	1	1.68×10^6	1.68×10^6	-6.21×10^3	1.98×10^4	1.67×10^6	1.70×10^6	2%
100	2	6.93×10^6	6.71×10^6	-4.69×10^4	3.17×10^5	6.88×10^6	7.03×10^6	2%
100	5	4.38×10^7	4.19×10^7	1.12×10^7	1.24×10^7	5.51×10^7	5.43×10^7	−1%
100	10	1.67×10^8	1.68×10^8	2.01×10^8	1.98×10^8	3.68×10^8	3.66×10^8	−1%
200	0.5	5.38×10^5	5.93×10^5	1.47×10^3	2.95×10^3	5.40×10^5	5.96×10^5	10%
200	1	2.39×10^6	2.37×10^6	1.43×10^4	4.71×10^4	2.40×10^6	2.42×10^6	1%
200	2	9.85×10^6	9.49×10^6	3.74×10^5	7.54×10^5	1.02×10^7	1.02×10^7	0%
200	5	6.14×10^7	5.93×10^7	3.18×10^7	2.95×10^7	9.31×10^7	8.88×10^7	−5%
200	10	2.34×10^8	2.37×10^8	4.56×10^8	4.71×10^8	6.89×10^8	7.09×10^8	3%
300	0.5	6.61×10^5	7.27×10^5	3.49×10^3	4.89×10^3	6.64×10^5	7.31×10^5	10%
300	1	2.93×10^6	2.91×10^6	4.43×10^4	7.83×10^4	2.98×10^6	2.98×10^6	0%
300	2	1.21×10^7	1.16×10^7	9.36×10^5	1.25×10^6	1.30×10^7	1.29×10^7	−1%
300	5	7.51×10^7	7.27×10^7	5.42×10^7	4.89×10^7	1.29×10^8	1.22×10^8	−6%
300	10	2.87×10^8	2.91×10^8	7.25×10^8	7.83×10^8	1.01×10^9	1.07×10^9	6%

cases considered, the model predictions for W_t agree with the MACH2 results to within 12%.

Comparing Eqs. (4) and (31), we find that in contrast to its nominal room-temperature value of 72 $\mu\Omega$-cm, the characteristic resistance of stainless steel at high current densities is 110 $\mu\Omega$-cm. Comparing Eqs. (12) and (32), we find that for the conditions studied herein, Eq. (12) is always greater than Eq. (32), as expected. For a current pulse that rises in 300 ns and peaks at 10 MA/cm, the loss predicted by Eq. (12) is 41% greater than that predicted by Eq. (32). The difference between Eqs. (12) and (32) exceeds 41% for the other cases considered.

Table I lists only the energy losses at peak current. We caution that the semianalytic estimates of $W_r + W_m$, $W_w + W_{\Delta L}$, and W_t are significantly less accurate at times when the current is less than half its peak value; i.e., early in time. However, at such times the losses are much less than at peak current, and for many cases of practical interest, are significantly less important.

V. MEASUREMENTS OF ENERGY LOSS TO STAINLESS-STEEL CONDUCTORS

Measurements of the total energy loss to a system of stainless-steel conductors operated at high lineal current densities were performed on four Z-accelerator shots [32]. The load for these shots was the conductor system itself, which was fielded at the center of the Z stack-MITL system. A cross-sectional view of the system is presented by Fig. 2. Two load configurations were used; these are outlined by Figs. 3 and 4. Both loads were low-inductance short circuits, which were designed to generate a low level

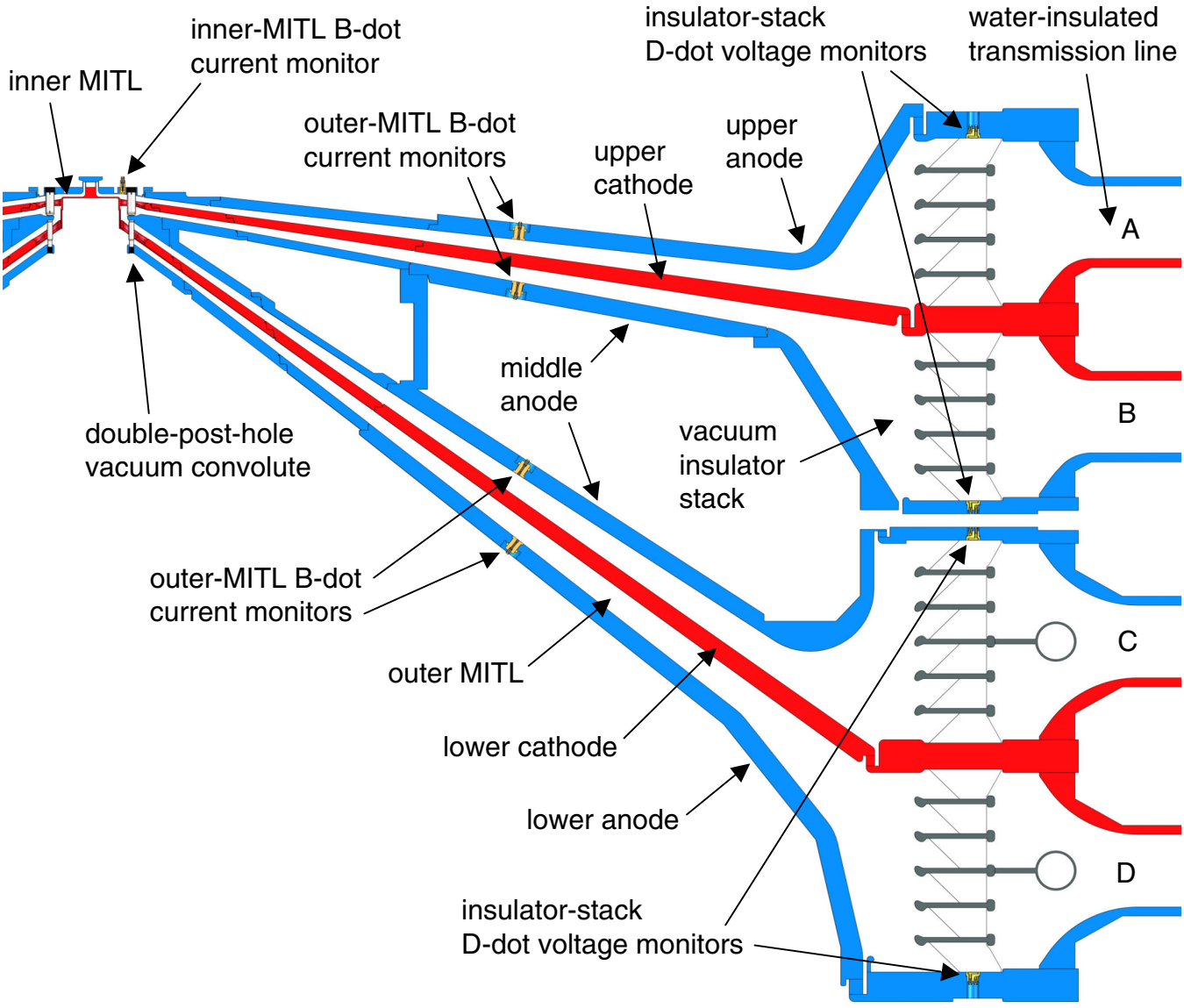

FIG. 2. (Color) Cross-sectional view of the vacuum-insulator stack and magnetically insulated transmission-line (MITL) system of the Z pulsed-power accelerator [1,2,4–10].

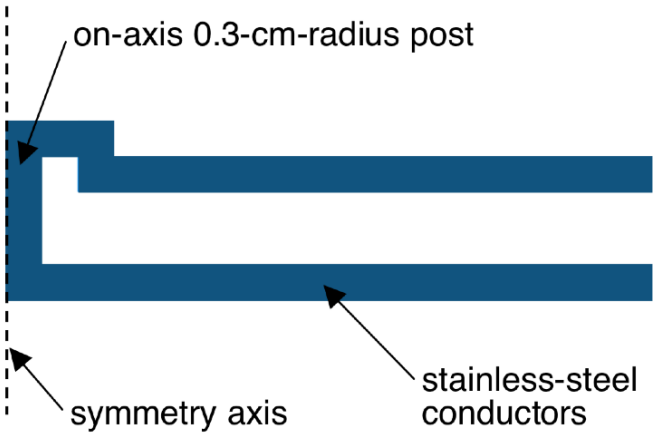

FIG. 3. (Color) Cross-sectional view of the system of stainless-steel conductors fielded as the load on Z-accelerator-shots 507, 532, and 589. The illustration is to scale. Except for the on-axis post, the conductors are 0.3-cm thick. The outer radius of the conductors is 5.38 cm.

of electron-flow current in the MITLs. Such loads were selected so that MITL effects would not obscure measurements of the conductor energy loss that is addressed by the present article.

The Z-shot numbers are 507, 532, 533, and 589. Shots 507, 532, and 589 used the load outlined by Fig. 3; shot 533 used the load of Fig. 4. The peak load currents on the shots were 21.3, 22.8, 24.3, and 21.9 MA, respectively. The corresponding *nominal* peak lineal current densities were 11.3, 12.1, 1.93, and 11.6 MA/cm. The times to peak current for these four shots were 107, 165, 169, and 109 ns. The pulse width for shots 532 and 533 was increased by closing the main water switches of the Z accelerator. The pulse was lengthened intentionally, to provide a more-meaningful test of the material constants β and κ.

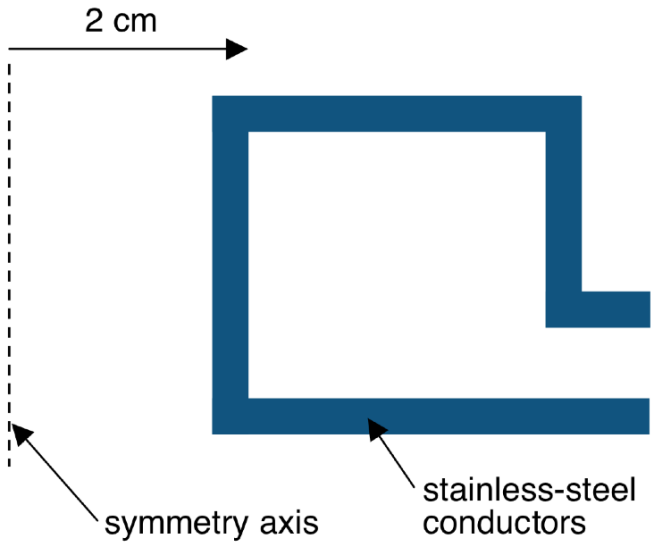

FIG. 4. (Color) Cross-sectional view of the system of stainless-steel conductors fielded as the load on Z-accelerator-shot 533. The illustration is to scale. The conductors are 0.3-cm thick; the outer radius of the conductors is 5.38 cm.

The conductor energy loss determined experimentally is estimated from the following expression:

$$\int_S W_{t,\mathrm{exp}}(t)dA = \int_0^t P_{\mathrm{stack}}dt - \left[\frac{1}{2}\sum_i L_i I_i^2 + \frac{1}{2}\sum_i C_i V_i^2 + \sum_t \int_0^t I_i^2 R_i dt + \int_0^t V_c I_c dt\right]. \quad (34)$$

The quantity P_{stack} is the total electrical power that flows into the stack-MITL system. The quantities L_i, C_i, and R_i are the inductance, capacitance, and resistance of the ith component of the system. The quantities I_i and V_i are the current and voltage at the ith component. The last term of Eq. (34) accounts for MITL flow electrons that are lost to the anode in the vicinity of the system's vacuum double-post-hole convolute [35–42]. All the currents and voltages on the right-hand side of Eq. (34) were measured using the differential-output B-dot and D-dot monitors that are described in Refs. [43,44]; a few of the monitors are depicted by Fig. 2.

For the shots described above, the Z MITL system was magnetically insulated very early in the pulse [2,4,9]. (The MITLs were designed to be insulated early, for loads of interest, to minimize the energy that is lost to electron-flow current [2,4,9].) Once insulation is established, most of the electron-flow current launched in the outer MITLs is lost in the vicinity of the convolute [37–42]. The lost current is accounted for by the final term on the right-hand side of Eq. (34). For the experiments described herein, this term does not exceed 2% of the total energy delivered to the stack-MITL system. The electron-flow current that originates in the inner MITL (which is located downstream of the convolute) is negligible [2,4,9].

The term on the right-hand side of Eq. (34) that includes R_i is summed over all the conductors located outside a 5.38-cm radius. We define this term to be that due to the energy loss to conductors operated at *low* lineal current densities. As discussed in Appendix A, we arbitrarily define the boundary between low and high current densities to be 0.63–0.72 MA/cm. We assume that for conductors outside a 5.38-cm radius, the sum of the Ohmic and diffusive losses is given by Eq. (4), and use the room-temperature resistivity for η. For conductors outside a 5.38-cm radius, the W_w and $W_{\Delta L}$ losses can be neglected.

VI. RESULTS

Figures 5–8 plot the measured energy loss as a function of time for each of the four Z-accelerator shots described in Sec. V. Also plotted is the energy loss predicted by the

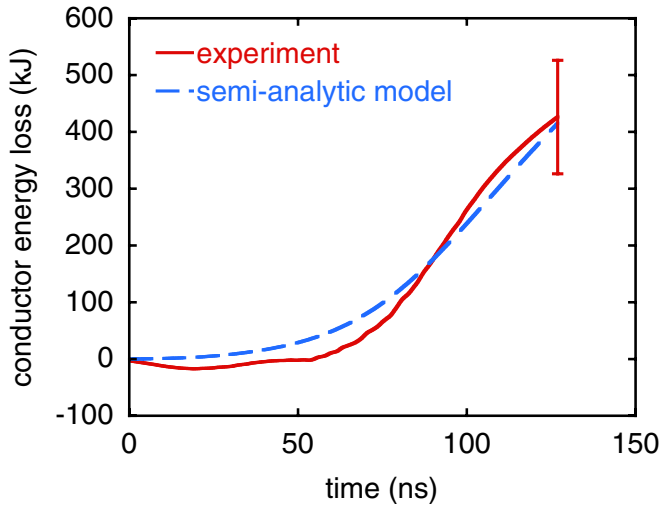

FIG. 5. (Color) Comparison of the measured conductor energy loss on Z-shot 507 with the prediction of the semianalytic model, as given by Eq. (35). The conductor system used as the load on this shot is that illustrated by Fig. 3. The plot includes a representative error bar.

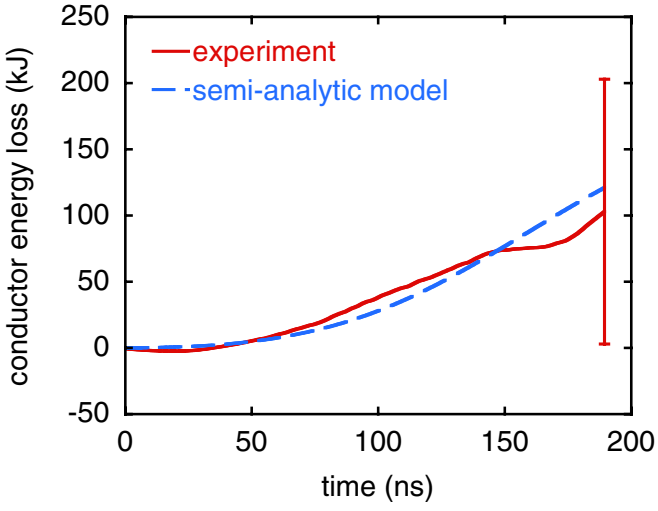

FIG. 7. (Color) Comparison of the measured conductor energy loss on Z-shot 533 with the prediction of the semianalytic model, as given by Eq. (35). The conductor system used as the load on this shot is that illustrated by Fig. 4. The plot includes a representative error bar.

semianalytic model, when expressed in terms of the effective resistance developed in Sec. III. For the conductor system used in the experiments, the effective resistance $R_{\rm eff}$ is given by the following expression:

$$R_{\rm eff} = 2\pi X_1 \frac{1}{t^{1/2}}\left[\sum_i\left(\frac{\ell_i}{a_i}\right) + \sum_j\left(\ln\frac{c_j}{b_j}\right)\right] + 2\pi X_2 t^{1/4} I^2(t)\left[\sum_i\left(\frac{\ell_i}{a_i^3}\right) + \frac{1}{2}\sum_j\left(\frac{1}{b_j^2} - \frac{1}{c_j^2}\right)\right], \quad (35)$$

where X_1 and X_2 are given by Eqs. (19), (20), and (25)–(30). The plots of Figs. 5–8 start at the extrapolated beginning of the load current, ignoring a small prepulse. The plots end 20 ns after peak current.

For each of the four shots, the total experimental uncertainty (due to random and systematic errors) in the measured value of the energy loss is estimated to be ± 100 kJ; hence, the excellent agreement between theory and experiment suggested by Figs. 5–8 must be considered fortuitous. Since the measurements have a large uncertainty, they are

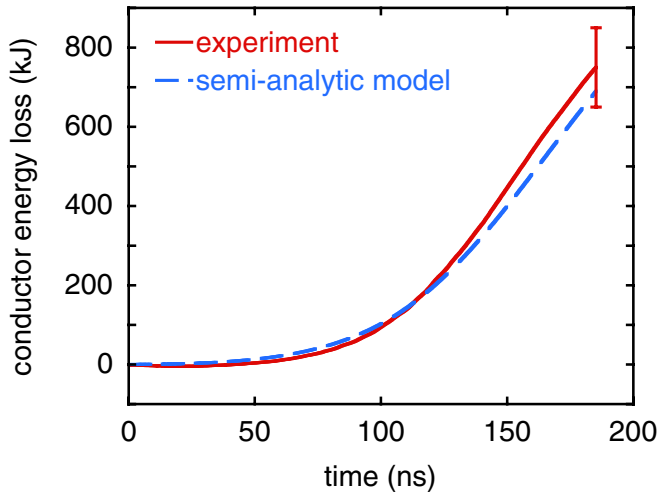

FIG. 6. (Color) Comparison of the measured conductor energy loss on Z-shot 532 with the prediction of the semianalytic model, as given by Eq. (35). The conductor system used as the load on this shot is that illustrated by Fig. 3. The plot includes a representative error bar.

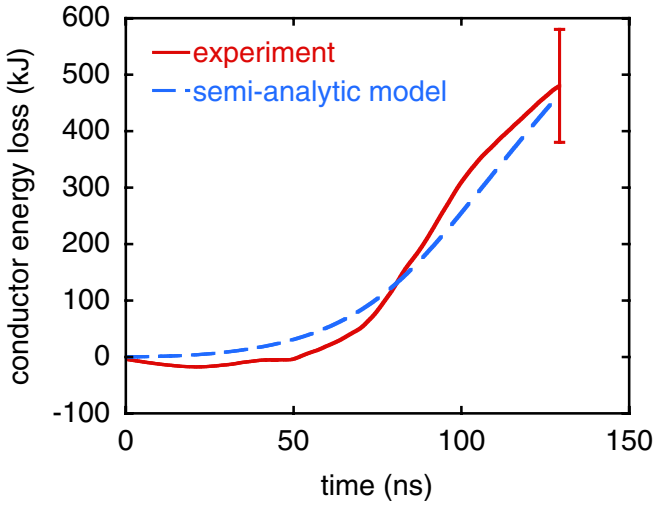

FIG. 8. (Color) Comparison of the measured conductor energy loss on Z-shot 589 with the prediction of the semianalytic model, as given by Eq. (35). The conductor system used as the load on this shot is that illustrated by Fig. 3. The plot includes a representative error bar.

TABLE II. Comparison of the conductor energy loss measured on Z-shots 507, 532, 533, and 589 with predictions of the semianalytic model, as expressed by Eq. (35). We also compare the measurements with predictions of a previously used conductor-loss model [Eq. (B3)]. The measurements validate Eq. (35) to zeroth order. The measurements also suggest that the previous model is significantly in error, and can predict losses that are too large by as much as an order of magnitude.

Z-shot number	Measured total energy loss W_t (kJ)	Total energy loss W_t predicted by the semianalytic model, Eq. (35) (kJ)	Total energy loss W_t predicted by the previous model, Eq. (B3) (kJ)
507	426 ± 100	415 ± 62	4870
532	750 ± 100	690 ± 104	6830
533	103 ± 100	121 ± 18	603
589	480 ± 100	466 ± 70	5420

useful only in demonstrating that Eq. (35) is consistent with experiment to zeroth order.

Table II compares, for each shot, the peak value of the measured energy loss to that predicted theoretically by the semianalytic model [Eq. (35)]. The table also compares the measurements to the predictions of an energy-loss model that was previously used by the pulsed-power community [45]; this model is outlined in Appendix B. Since the measurements have large uncertainties, they only validate Eq. (35) to zeroth order. However, the measurements exclude the possibility that the previous model [Eq. (B3)] is correct. In fact, the previous model predicts that for Z shots 507, 532, and 589, the energy loss is a factor of 1.7–2.0 greater than the total energy delivered to the Z stack-MITL system; hence, it is clear that the previous model is significantly in error.

The comparisons made by Figs. 5–8 and Table II implicitly assume that the 1D-planar approximation applies to the experiments. This assumption is examined in Appendix C. The comparisons also assume that the time history of the load current can be approximated by a linear ramp; this assumption is examined in Appendix D.

VII. SUGGESTIONS FOR FUTURE WORK

The analytic results developed in Secs. II and III assume that the current time history can be approximated as a linear ramp. As mentioned previously, analytic results for other power-law functions can be obtained using the procedure outlined herein.

The MHD simulations described in Sec. IV were performed using the MACH2 code [28,30,31]. It would be of interest to repeat the simulations described in Sec. IV with other MHD codes, to determine whether they give comparable results.

As discussed in Sec. IV, Eqs. (13) and (14) were normalized to the results of MACH2 simulations that assume a linear-ramp current pulse is applied to a 1-cm-radius stainless-steel cylinder. If desired, one could assume a current time history that deviates slightly from a linear ramp, a different conductor geometry, and a different conductor material, to obtain results more relevant to a problem at hand. Doing so would, of course, result in a different set of material constants α, β, γ, ζ, κ, and λ.

The energy-loss measurements discussed in Sec. V were performed by taking the difference of two quantities that are similar in magnitude; hence, the measured losses have a large uncertainty. Such uncertainties could be reduced by designing an experimental arrangement considerably simpler than that indicated by Fig. 2, without a double-post-hole vacuum convolute, and with more current and voltage measurements performed closer to the high-lineal-current-density conductors under study. It would also be of interest to measure energy loss to conductors other than stainless steel, and to compare such measurements with predictions.

ACKNOWLEDGMENTS

The authors gratefully acknowledge W. Ballard, J. Barth, W. Beezhold, T. Bock, J. Boyes, E. Breden, R. Brockman, R. Broyles, P. Corcoran, M. Cuneo, D. Dalton, T. Dinwoodie, J. Douglas, S. Downie, D. Droemer, M. Dudley, S. Frese, J. Gergel, J. Gergel, Jr., C. Guthrie, R. Hanes-Michaud, E. Harlan, M. Harris, D. Heath, M. Herrmann, D. Jobe, K. Jones, J. Kellogg, M. Kernaghan, A. Kim, J. Lee, R. Leeper, G. Leifeste, F. Long, J. Lynch, M. K. Matzen, M. Mazarakis, D. McDaniel, J. McKenney, J. Melville, L. P. Mix, J. Moore, W. Moore, R. Mourning, G. Mowrer, T. Mulville, M. Pelock, D. Petmecky, B. Peyton, S. Ploor, J. Porter, J. Powell, J. Puissant, J. Ramirez, L. Reynolds, D. Rice, C. Robinson, G. A. Rochau, G. E. Rochau, M. Roderick, T. Romero, R. Ross, D. Sachs, R. Sachs, M. Savage, L. Schneider, J. F. Seamen, J. H. Seamen, J. Serrano, A. Seth, A. Sharpe, W. R. Shoup, W. Simpson, J. Slopek, I. Smith, J. Smith, R. Starbird, M. Sullivan, D. Van De Valde, D. Walsh, E. Walsh, M. Walsh, J. Webb, L. Wilson, R. Woodring, and M. York, and our many other colleagues at Barth Electronics, C-Lec Plastics, EG&G, Ktech Corporation, L-3 Communications, Los Alamos National Laboratory, NumerEx, Prodyn Technologies, Sandia

National Laboratories, Team Specialty Products, T&M Research Products, Voss Scientific, and Votaw Precision Technologies, for invaluable contributions. Sandia is a multiprogram laboratory operated by Sandia Corporation, a Lockheed Martin Company, for the United States Department of Energy's National Nuclear Security Administration under Contract No. DE-AC04-94AL85000.

APPENDIX A: LOW LINEAL CURRENT DENSITIES

At sufficiently *low* lineal-current densities, the contribution of the sum $W_w + W_{\Delta L}$ to W_t [Eq. (1)] can be neglected, and W_t may be approximated by Eq. (4) with η set equal to the room-temperature resistivity. Consequently, in circuit simulations of the operation of a pulsed-power accelerator, we estimate the energy loss to conductors operated at *low* current densities by using an expression for the effective resistance $R_{\rm eff}$ that derives from Eq. (4). At *high* current densities we use Eqs. (21)–(24).

For the measurements discussed in Sec. V, we *arbitrarily* define the boundary between low and high lineal current densities to be that where the peak current density reaches 0.63–0.72 MA/cm (which correspond to 79–90 T magnetic fields). This choice is motivated by the geometry of the Z MITL system, and simplifies the measurements discussed in Sec. V. It is clear that a more numerically correct approach could be used; the development of such an approach is outside the scope of this article. For many cases of practical interest, the results obtained are insensitive to the exact choice of the field used to define the boundary.

Fields of 79–90 T are comparable to the "critical magnetic field" B_c defined by Knoepfel [21,22]. The critical field is that which causes the resistivity at the surface of a conductor *nominally* to double. According to Ref. [21], the value of B_c for stainless steel is 97 T (which corresponds to 0.77 MA/cm). This value is estimated using the approach described in Sec. 4.23 of Ref. [21], which assumes $I(t) \propto t^{1/2}$.

We calculate B_c here taking a slightly different approach, and assume instead that $I(t) \propto t$. Following Knoepfel [Eqs. (10.69) and (10.70) of Ref. [21]], we assume that at sufficiently low temperatures (i.e., low lineal current densities), the time-dependent resistivity of the surface of a conductor $\eta(t)$ is given by

$$\eta(t) = \eta_0[1 + \beta c_v(\Delta\theta)], \tag{A1}$$

where η_0 is the room-temperature resistivity, β is the heat coefficient of resistivity [21], c_v is the specific heat per unit volume, and $\Delta\theta$ is the temperature change at the conductor surface. (The quantity β used in this Appendix is, of course, not the material constant used in the main body of this article.)

According to Eq. (4.38) of Ref. [21],

$$\Delta\theta = \frac{\vartheta B^2(t)}{2\mu_0 c_v}, \tag{A2}$$

where ϑ is the dimensionless surface energy factor defined in Sec. 4.12 of Ref. [21], and $B(t)$ is the magnetic field at the surface of the conductor. Combining Eqs. (A1) and (A2) gives

$$\eta(t) = \eta_0\left(1 + \frac{\beta\vartheta B^2(t)}{2\mu_0}\right). \tag{A3}$$

For stainless steel,

$$\eta_0 = 72 \times 10^{-8}\ \Omega\text{-m}, \tag{A4}$$

$$\beta = 2.67 \times 10^{-10}\ \text{m}^3/\text{J}, \tag{A5}$$

$$c_v = 3.37 \times 10^6\ \text{J/m}^3\text{-K}. \tag{A6}$$

The values of β and c_v given above are those averaged over the interval from 0 to 1000 C, and are deduced from information presented in Ref. [21]. When $I(t) \propto t$ then according to Table 4.II of [21]

$$\vartheta = 1.273. \tag{A7}$$

According to Eq. (A3), η increases a factor of 2 when

$$B(t) = B_c \equiv \left(\frac{2\mu_0}{\vartheta\beta}\right)^{1/2}. \tag{A8}$$

Equations (A5), (A7), and (A8) suggest that the resistivity of a stainless-steel conductor increases nominally a factor of 2 when $B(t) = B_c = 86$ T. This field differs from that calculated by Knoepfel by the factor $\vartheta^{-1/2}$.

It is clear that our elementary approach to modeling energy loss is not accurate for conductors at which the peak current density is on the order of B_c; however, for many cases of experimental interest, the loss to such conductors is not a significant fraction of the total energy in the system.

APPENDIX B: PREVIOUS MODEL OF ENERGY LOSS TO CONDUCTORS OPERATED AT HIGH LINEAL CURRENT DENSITIES

This Appendix outlines a previously used model of conductor energy loss [45]. The model assumes

$$W_t \propto t^{1/2}B^3(t). \tag{B1}$$

The model predicts that the effective resistance of a *pair* of identical horizontal-disk *copper* electrodes (with an infinitely large outer radius) is given by the following expression:

TABLE III. Summary of conductor-energy-loss calculations performed to quantify the accuracy of the 1D-planar approximation. These assume a linear-ramp current pulse is applied to a 0.3-cm-radius solid cylinder of stainless steel. The numerical results are obtained from a 1D Lagrangian MHD simulation performed using the MACH2 code [28,30,31]. The losses presented here are those obtained at peak current. As suggested below, the total energy loss W_t given by Eq. (33) agrees to first order with the simulation result.

Time to peak current (ns)	Peak nominal lineal current density (MA/cm)	$W_r + W_m$ (MACH2) (J/m^2)	$W_r + W_m$ [Eq. (31)] (J/m^2)	$W_w + W_{\Delta L}$ (MACH2) (J/m^2)	$W_w + W_{\Delta L}$ [Eq. (32)] (J/m^2)	W_t (MACH2) (J/m^2)	W_t [Eq. (33)] (J/m^2)	Difference between the semianalytic and MACH2 estimates of W_t
150	12	3.11×10^8	2.96×10^8	7.29×10^8	6.82×10^8	1.04×10^9	9.78×10^8	−6%

$$R_{\text{eff}}(t) = (3 \times 10^{-15}) \frac{I(t)}{b\, t^{1/2}}, \tag{B2}$$

where b is the inner radius of the electrodes. Equation (B2) was incorporated into the SCREAMER circuit code, and is presented on pages 3–13 of the 1995 SCREAMER user's manual [45].

Equations (16)–(23), (B1), and (B2) suggest that, for a system of cylindrical and disk-shaped electrodes, Eq. (B2) is generalized as follows:

$$R_{\text{eff}} = (1.5 \times 10^{-15}) \frac{I(t)}{t^{1/2}} \left[\sum_i \frac{\ell_i}{a_i^2} + \sum_j \sec\vartheta_j \left(\frac{1}{b_j} - \frac{1}{c_j} \right) \right]. \tag{B3}$$

We use Eq. (B3) to predict the conductor energy loss for the experiments described in Sec. V; the predictions are listed in Table II.

Equation (B3) assumes copper conductors, whereas the experiments of Sec. V used stainless steel. Since the high-temperature resistivity and room-temperature mass density of copper are comparable to those of stainless, Eqs. (4) and (12) suggest that if Eq. (B3) were correct, it would predict losses that are comparable to the observed values. Instead, as suggested by Table II, Eq. (B3) predicts losses that are as much as *an order of magnitude greater*. In fact, for Z shots 507, 532, and 589, Eq. (B3) predicts losses that are a factor of 1.7–2.0 greater than the total energy delivered to the Z-accelerator stack-MITL system. Hence, it appears Eq. (B3) is significantly in error, and predicts losses that can be too large by as much as an order of magnitude.

APPENDIX C: VERIFICATION THAT THE 1D-PLANAR ASSUMPTION APPLIES TO THE EXPERIMENTS

The semianalytic model developed in Secs. II and III assumes that the current-density and magnetic-field profiles in the conductor can be approximated as one-dimensional and planar. The MHD simulations discussed in Sec. IV assume that the current is carried by a 1-cm-radius solid cylinder of stainless steel, since such a system is approximately 1D and planar (given the millimeter-scale resistive skin depth of our 50–300 ns ramped currents), and since such a geometry is likely to be that of most interest for future systems that drive a z-pinch load.

However, the stainless-steel electrodes of Fig. 3 include a 0.3-cm-radius conductor on axis. The radius was chosen to be this small to achieve on Z a current density on the order of 10 MA/cm. In Sec. VI, we compare measurements made with the electrodes of Fig. 3 to the predictions of the semianalytic model. To determine whether the 1D-planar approximation is applicable when the minimum radius is 0.3 cm, we performed a 1D Lagrangian MACH2 simulation that assumes a current pulse with a peak nominal lineal current density of 12 MA/cm, and a 150-ns rise time, is applied to a 0.3-cm-radius stainless cylinder.

The results of the simulation are presented in Table III, along with the predictions of the semianalytic model. It appears that the model is, in fact, applicable to a conductor with such a small radius, under the conditions studied. However, we caution that the agreement indicated by Table III is due, in part, to compensating effects.

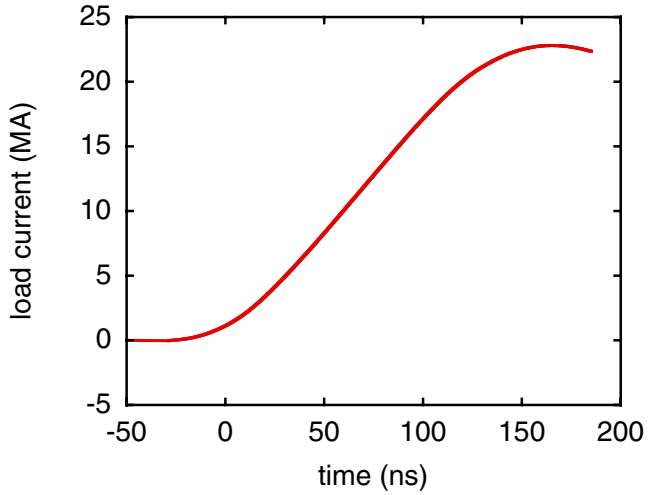

FIG. 9. (Color) Measured load current on Z-shot 532. The current time history deviates significantly from an ideal linear ramp for times greater than 130 ns. The plot ends at time $t = 185$ ns, 20 ns after peak current.

TABLE IV. Summary of conductor-energy-loss calculations performed to quantify the accuracy of the linear-ramp assumption. The 5th column presents results of 1D-Lagrangian MACH2 simulations that use the load-current time history as measured on Z-shot 532 (instead of a linear ramp); this current is plotted by Fig. 9. The 6th column presents energy-loss estimates obtained using Eq. (22) [together with Eqs. (25)–(30) and (D1)] and the current time history plotted by Fig. 9. (The current of Fig. 9 was scaled by a factor of 2.755 for the 62.8-MA calculations.) For the first three cases considered, the calculations were performed until time $t = 185$ ns (i.e., 20 ns after peak current); for the fourth case, until $t = 165$ ns (peak current). As suggested by the last two rows, the agreement between Eq. (22) and MACH2 improves at times less than 185 ns (as the pulse shape becomes more like a linear ramp), which is consistent with the results presented by Table I (which assumes an exact linear ramp).

Peak current	Initial radius of the stainless-steel cylinder (cm)	Peak nominal lineal current density (MA/cm)	Time to which the calculations are performed (ns)	W_t (MACH2) (J/m^2)	W_t [as determined using Eq. (22)] (J/m^2)	Difference between the semianalytic and MACH2 estimates of W_t
22.8 MA	0.3	12	185	2.11×10^9	2.31×10^9	9%
22.8 MA	1.0	3.6	185	5.61×10^7	6.14×10^7	9%
62.8 MA	1.0	10	185	9.58×10^8	1.19×10^9	24%
62.8 MA	1.0	10	165	7.75×10^8	8.95×10^8	16%

APPENDIX D: VERIFICATION THAT THE LINEAR-RAMP ASSUMPTION APPLIES TO THE EXPERIMENTS

The semianalytic model developed in Secs. II and III assumes that the current time history is a linear ramp. However, the actual time histories of the experiments described herein resemble that plotted by Fig. 9, which is the measured load current on Z-accelerator shot 532.

To determine whether the linear-ramp assumption is applicable to waveforms similar to that plotted by Fig. 9, we performed four 1D-Lagrangian MACH2 simulations that use the measured Z-shot-532 load-current time history, instead of a linear ramp. The simulations apply the current to a solid stainless-steel cylinder. The results of the simulations are summarized by Table IV. For the 62.8-MA simulations, the current of Fig. 9 is scaled by a factor of 2.755.

Also summarized by Table IV are predictions of Eq. (22) [when used with Eqs. (25)–(30)] and the following expression:

$$W_t = \frac{\int I^2 R_{\text{eff}} dt}{S}, \tag{D1}$$

where S is the initial surface area of the stainless-steel cylinder. In the above expression $I(t)$ is assumed to have the pulse shape plotted by Fig. 9, instead of a linear ramp. The effective resistance is taken to be that given by Eq. (22) (which, of course, is derived assuming a linear ramp.) As above, for the 62.8-MA calculations, the current of Fig. 9 is scaled by a factor of 2.755.

For each of the four cases considered, the semianalytic model [when expressed as Eq. (22)] agrees with MACH2 to within 24%. The plot of Fig. 9 extends to 185 ns. For the first three cases considered, the calculations were performed until time $t = 185$ ns (i.e., until 20 ns after peak current); for the fourth case, until $t = 165$ ns (peak current). As suggested by the last two rows, the agreement between Eq. (22) and MACH2 improves at times less than 185 ns (as the pulse shape becomes more like a linear ramp), which is consistent with the results presented by Table I (which assumes an exact linear ramp).

[1] R. B. Spielman, W. A. Stygar, J. F. Seamen, F. Long, H. Ives, R. Garcia, T. Wagoner, K. W. Struve, M. Mostrom, I. Smith, P. Spence, and P. Corcoran, in *Proceedings of the 11th IEEE International Pulsed Power Conference*, edited by G. Cooperstein and I. Vitkovitsky (IEEE, Piscataway, NJ, 1997), p. 709.

[2] P. A. Corcoran, J. W. Douglas, I. D. Smith, P. W. Spence, W. A. Stygar, K. W. Struve, T. H. Martin, R. B. Spielman, and H. C. Ives, in Proceedings of the 11th IEEE International Pulsed Power Conference (Ref. [1]), p. 466.

[3] R. J. Garcia, H. C. Ives, K. W. Struve, R. B. Spielman, T. H. Martin, M. L. Horry, R. Wavrik, and T. F. Jaramillo, in Proceedings of the 11th IEEE International Pulsed Power Conference (Ref. [1]), p. 1614.

[4] H. C. Ives, D. M. Van De Valde, F. W. Long, J. W. Smith, R. B. Spielman, W. A. Stygar, R. W. Wavrick, and R. W. Shoup, in Proceedings of the 11th IEEE International Pulsed Power Conference (Ref. [1]), p. 1602.

[5] M. A. Mostrom, T. P. Hughes, R. E. Clark, W. A. Stygar, and R. B. Spielman, in Proceedings of the 11th IEEE International Pulsed Power Conference (Ref. [1]), p. 460.

[6] R. W. Shoup, F. Long, T. H. Martin, R. B. Spielman, W. A. Stygar, M. A. Mostrom, K. W. Struve, H. Ives, P. Corcoran, and I. Smith, in Proceedings of the 11th IEEE International Pulsed Power Conference (Ref. [1]), p. 1608.

[7] I. D. Smith, P. A. Corcoran, W. A. Stygar, T. H. Martin, R. B. Spielman, and R. W. Shoup, in Proceedings of the 11th IEEE International Pulsed Power Conference (Ref. [1]), p. 168.

[8] K. W. Struve, T. H. Martin, R. B. Spielman, W. A. Stygar, P. A. Corcoran, and J. W. Douglas, in Proceedings of the 11th IEEE International Pulsed Power Conference (Ref. [1]), p. 162.

[9] W. A. Stygar, R. B. Spielman, G. O. Allshouse, C. Deeney, D. R. Humphreys, H. C. Ives, F. W. Long, T. H. Martin, M. K. Matzen, D. H. McDaniel, C. W. Mendel, Jr., L. P. Mix, T. J. Nash, J. W. Poukey, J. J. Ramirez, T. W. L. Sanford, J. F. Seamen, D. B. Seidel, J. W. Smith, D. M. Van De Valde, R. W. Wavrik, P. A. Corcoran, J. W. Douglas, I. D. Smith, M. A. Mostrom, K. W. Struve, T. P. Hughes, R. E. Clark, R. W. Shoup, T. C. Wagoner, T. L. Gilliland, and B. Peyton, in Proceedings of the 11th IEEE International Pulsed Power Conference, Baltimore (Ref. [1]), p. 591.

[10] R. B. Spielman, C. Deeney, G. A. Chandler, M. R. Douglas, D. L. Fehl, M. K. Matzen, D. H. McDaniel, T. J. Nash, J. L. Porter, T. W. L. Sanford, J. F. Seamen, W. A. Stygar, K. W. Struve, S. P. Breeze, J. S. McGurn, J. A. Torres, D. M. Zagar, T. L. Gilliland, D. O. Jobe, J. L. McKenney, R. C. Mock, M. Vargas, T. Wagoner, and D. L. Peterson, Phys. Plasmas **5**, 2105 (1998).

[11] W. A. Stygar, M. E. Cuneo, D. I. Headley, H. C. Ives, R. J. Leeper, M. G. Mazarakis, C. L. Olson, J. L. Porter, T. C. Wagoner, and J. R. Woodworth, Phys. Rev. ST Accel. Beams **10**, 030401 (2007).

[12] J. M. Creedon, J. Appl. Phys. **46**, 2946 (1975).

[13] J. M. Creedon, J. Appl. Phys. **48**, 1070 (1977).

[14] M. S. Di Capua, IEEE Trans. Plasma Sci. **11**, 205 (1983).

[15] C. W. Mendel, Jr., D. B. Seidel, and S. E. Rosenthal, Laser Part. Beams **1**, 311 (1983).

[16] W. A. Stygar, T. C. Wagoner, H. C. Ives, P. A. Corcoran, M. E. Cuneo, J. W. Douglas, T. L. Gilliland, M. G. Mazarakis, J. J. Ramirez, J. F. Seamen, D. B. Seidel, and R. B. Spielman, Phys. Rev. ST Accel. Beams **9**, 090401 (2006).

[17] J. H. Hammer, M. Tabak, S. C. Wilks, J. D. Lindl, D. S. Bailey, P. W. Rambo, A. Toor, G. B. Zimmerman, and J. L. Porter, Jr., Phys. Plasmas **6**, 2129 (1999).

[18] M. E. Cuneo, R. A. Vesey, D. B. Sinars, J. P. Chittenden, E. M. Waisman, R. W. Lemke, S. V. Lebedev, D. E. Bliss, W. A. Stygar, J. L. Porter, D. G. Schroen, M. G. Mazarakis, G. A. Chandler, and T. A. Mehlhorn, Phys. Rev. Lett. **95**, 185001 (2005).

[19] W. A. Stygar, M. E. Cuneo, R. A. Vesey, H. C. Ives, M. G. Mazarakis, G. A. Chandler, D. L. Fehl, R. J. Leeper, M. K. Matzen, D. H. McDaniel, J. S. McGurn, J. L. McKenney, D. J. Muron, C. L. Olson, J. L. Porter, J. J. Ramirez, J. F. Seamen, C. S. Speas, R. B. Spielman, K. W. Struve, J. A. Torres, E. M. Waisman, T. C. Wagoner, and T. L. Gilliland, Phys. Rev. E **72**, 026404 (2005).

[20] R. A. Vesey, M. C. Herrmann, R. W. Lemke, M. P. Desjarlais, M. E. Cuneo, W. A. Stygar, G. R. Bennett, R. B. Campbell, P. J. Christenson, T. A. Mehlhorn, J. L. Porter, and S. A. Slutz, Phys. Plasmas **14**, 056302 (2007).

[21] H. Knoepfel, *Pulsed High Magnetic Fields* (North-Holland, London, 1970).

[22] H. E. Knoepfel, *Magnetic Fields* (Wiley, New York, 2000).

[23] S. Singer and R. O. Hunter, in *Proceedings of the 3rd International Pulsed Power Conference*, edited by T. H. Martin and A. H. Guenther (IEEE, New York, 1981), p. 351.

[24] *Electrical Resistivity Handbook*, edited by G. T. Dyos and T. Farrell (Peter Peregrinus, London, 1992).

[25] A. W. DeSilva and J. D. Katsouros, Phys. Rev. E **57**, 5945 (1998).

[26] S. E. Rosenthal, M. P. Desjarlais, R. B. Spielman, W. A. Stygar, J. R. Asay, M. R. Douglas, C. A. Hall, M. H. Frese, R. L. Morse, and D. B. Reisman, IEEE Trans. Plasma Sci. **28**, 1427 (2000).

[27] *High Voltage Vacuum Insulation*, edited by R. V. Latham (Academic, San Diego, 1995).

[28] *MACH2: A Two-dimensional Magnetohydrodynamic Simulation Code for Complex Experimental Configurations*, edited by M. H. Frese (NumerEx, Albuquerque, NM, 1990), www.numerex-llc.com.

[29] R. B. Spielman, S. Chantrenne, and D. H. McDaniel, in *Proceedings of the 16th IEEE International Pulsed Power Conference*, edited by E. Schamiloglu and F. Peterkin (IEEE, Piscataway, NJ, 2007), p. 937.

[30] M. P. Desjarlais, Contrib. Plasma Phys. **41**, 267 (2001).

[31] K. S. Holian, LANL Report No. LA-10160-MS, 1984.

[32] W. A. Stygar, R. B. Spielman, G. O. Allshouse, M. R. Douglas, D. H. McDaniel, E. J. McGuire, S. E. Rosenthal, K. W. Struve, J. R. Asay, C. A. Hall, M. A. Bernard, D. B. Reisman, A. Toor, T. C. Wagoner, T. L Gilliland, and P. G. Reynolds, Bull. Am. Phys. Soc. **43**, 1904 (1998).

[33] D. E. Parks and P. W. Spence (unpublished).

[34] S. E. Rosenthal *et al.* (to be published).

[35] D. H. McDaniel, R. W. Stinnett, and I. D. Smith, Bull. Am. Phys. Soc. **25**, 1017 (1980).

[36] R. B. Spielman, P. Corcoran, J. Fockler, H. Kishi, and P. W. Spence, in *Proceedings of the 7th IEEE International Pulsed Power Conference*, edited by B. H. Bernstein and J. P. Shannon (IEEE, Piscataway, NJ, 1989), p. 445.

[37] T. P. Hughes and R. E. Clark, Mission Research Corporation Report No. MRC/ABQ-R-1875, 1998.

[38] T. P. Hughes and R. E. Clark, Mission Research Corporation Report No. MRC/ABQ-R-2005, 2000.

[39] T. P. Hughes, R. E. Clark, B. V. Oliver, R. A. St. John, and W. A. Stygar, Mission Research Corporation Report No. MRC/ABQ-R-2066, 2002.

[40] T. D. Pointon, W. A. Stygar, R. B. Spielman, H. C. Ives, and K. W. Struve, Phys. Plasmas **8**, 4534 (2001).

[41] D. V. Rose, D. R. Welch, T. P. Hughes, R. E. Clark, C. B. Mostrom, and W. A. Stygar, in *Proceedings of the 16th IEEE International Pulsed Power Conference*, edited by E. Schamiloglu and F. Peterkin (IEEE, Piscataway, NJ, 2007), p. 171.

[42] D. V. Rose, D. R. Welch, T. P. Hughes, R. E. Clark, and W. A. Stygar, Phys. Rev. ST Accel. Beams **11**, 060401 (2008).

[43] W. A. Stygar, R. B. Spielman, H. C. Ives, W. B. S. Moore, J. F. Seamen, A. W. Sharpe, T. C. Wagoner, T. L. Gilliland, R. S. Broyles, J. A. Mills, T. A. Dinwoodie, J. S. Slopek, K. W. Struve, and P. G. Reynolds, in Proceedings of the 11th IEEE International Pulsed Power Conference (Ref. [1]), p. 1258.

[44] T. C. Wagoner, W. A. Stygar, H. C. Ives, T. L. Gilliland, R. B. Spielman, M. F. Johnson, P. G. Reynolds, J. K. Moore, R. L. Mourning, D. L. Fehl, K. E. Androlewicz, J. E. Bailey, R. S. Broyles, T. A. Dinwoodie, G. L. Donovan, M. E. Dudley, K. D. Hahn, A. A. Kim, J. R.

Lee, R. J. Leeper, G. T. Leifeste, J. A. Melville, J. A. Mills, L. P. Mix, W. B. S. Moore, B. P. Peyton, J. L. Porter, G. A. Rochau, G. E. Rochau, M. E. Savage, J. F. Seamen, J. D. Serrano, A. W. Sharpe, R. W. Shoup, J. S. Slopek, C. S. Speas, K. W. Struve, D. M. Van De Valde, and R. M. Woodring, Phys. Rev. ST Accel. Beams **11**, 100401 (2008).

[45] The origin and development of the previously used conductor-energy-loss model are unclear. The model was incorporated into the SCREAMER circuit code in 1995. Equation (B2) is presented on pages 3–13 of SCREAMER, A Pulsed Power Design Tool, User's Guide for Version 2.0 (25 August 1995).